**OPEN**

# Injection- Seeded Optoplasmonic Amplifier in the Visible

Manas Ranjan Gartia[1,7], Sujin Seo[2,7], Junhwan Kim[3], Te-Wei Chang[4,7], Gaurav Bahl[3,4,7], Meng Lu[5], Gang Logan Liu[4,6,7] & J. Gary Eden[2,4,7]

[1]Department of Nuclear, Plasma and Radiological Engineering, University of Illinois at Urbana-Champaign, Urbana, IL 61801, USA, [2]Department of Materials Science and Engineering, University of Illinois at Urbana-Champaign, Urbana, IL 61801, USA, [3]Department of Mechanical Science and Engineering, University of Illinois at Urbana-Champaign, Urbana, IL 61801, USA, [4]Department of Electrical and Computer Engineering, University of Illinois at Urbana-Champaign, Urbana, IL 61801, USA, [5]Department of Electrical and Computer Engineering, Iowa State University, Ames, Iowa 50011, USA, [6]Department of Bioengineering, University of Illinois at Urbana-Champaign, Urbana, IL 61801, USA, [7]Micro and Nano Technology Laboratory, University of Illinois at Urbana-Champaign, Urbana, IL 61801, USA.

A hybrid optoplasmonic amplifier, injection-seeded by an internally-generated Raman signal and operating in the visible (563–675 nm), is proposed and evidence for amplification is presented. Comprising a gain medium tethered to a whispering gallery mode (WGM) resonator with a protein, and a plasmonic surface, the optical system described here selectively amplifies a single (or a few) Raman line(s) produced within the WGM resonator and is well-suited for routing narrowband optical power on-a-chip. Over the past five decades, optical oscillators and amplifiers have typically been based on the buildup of the field from the spontaneous emission background. Doing so limits the temporal coherence of the output, lengthens the time required for the optical field intensity to reach saturation, and often is responsible for complex, multiline spectra. In addition to the spectral control afforded by injection-locking, the effective Q of the amplifier can be specified by the bandwidth of the injected Raman signal. This characteristic contrasts with previous WGM-based lasers and amplifiers for which the Q is determined solely by the WGM resonator.

I n descending the spatial scale from the bulk crystals and discrete mirrors of the first lasers in 1960[1,2] to a single biological cell[3], quantum dots[4], or nanoparticles[5], optical oscillators and amplifiers have generally relied upon the growth of the optical field from the noise (e.g., spontaneous emission). Doing so, however, often restricts the temporal coherence of the output and unnecessarily extends the field buildup time which is a factor critical to several high-speed applications of pulsed systems. At the nano-/micro-scale, provisions for mode selection are often not available and the laser spectral output is typically complex, comprising numerous lines extending over a substantial portion of the gain medium bandwidth[5–8]. Such dense, multiline laser spectra are a decided drawback for applications including on-chip communications, computing, or biomedical sensing. Furthermore, micro/nano lasers and amplifiers have frequently combined the gain medium with the resonator[6–11]. Although tempting from the perspective of minimizing the overall volume of the emitter, integrating the two precludes the opportunity to optimize separately the performance of either element of the source. This is particularly true for crystalline microresonators[12,13] for which controllable doping of the resonator material with the lasant species is problematic.

An optoplasmonic amplifier, operating in the visible (563–675 nm) and injection-seeded by an internally-generated Raman signal, is introduced here and evidence of optical gain is presented. Dye molecules, tethered to the surface of a spherical microresonator by a protein, provide optical gain for the Raman (Stokes) radiation generated within the whispering gallery mode (WGM) resonator, or from another amplifier component (tether protein, Si substrate), by a laser (632.8 or 532 nm) pump source. Although the gain medium is located external to, and surrounds, the resonator, it lies well within the evanescent optical field of the sphere and, therefore, specific WGMs associated with the spherical resonator harvest energy efficiently from the optically-pumped dye molecules. Suspending the gain medium approximately 11 nm from the microresonator surface minimizes nonradiative quenching of electronically-excited dye molecules[14], and is found to double the excited state lifetime (relative to its value in solution). Because the amplifier output does not build up from the noise, the coincidence of the Raman seed radiation with a particular resonator mode has the effect of discriminating against all other modes, thereby providing control over the output spectrum. With judicious choice of the amplifier parameters, the energy stored under the amplifier gain profile is extracted predominantly in a single line by

injection-locking[15–19] because the medium is homogeneously-broadened. Power is coupled into, and out of, the spherical resonator by a nanoantenna (plasmonic) array on which the microresonator rests. Because of its contact with a portion of the microresonator surface, the plasmonic network also serves to strengthen the local electric field inside the microresonator, thereby enhancing the generation of the Stokes seed radiation. If the dye is removed from the periphery of the spherical resonator and, instead, is situated at the interface between the resonator and the plasmonic array, optical amplification of specific Raman lines ceases, and a conventional, surface-enhanced Raman scattering (SERS) spectrum of the dye alone is observed. Owing to the narrow linewidth of the injection seed that is available with Raman scattering, and the potential for energy storage in the gain medium surrounding the resonator, the coherence and output power of this visible emitter can be superior to those of existing nano/micro optical sources. Specifically, the effective Q of the amplifier can be determined by the bandwidth of the injected Raman signal, in contrast to previous WGM-based lasers and amplifiers in which the optical field builds up from the noise and the Q of an oscillator is dependent entirely upon the resonator. The compound photonic-plasmonic device reported here provides an optical system suited for parallel, distributed systems designed for storing, amplifying, and routing optical power on a chip or within scattering media.

Precise manipulation of light at the micro- and nano-spatial scales is a prerequisite to realizing physical analogs of optical processes in nature, such as photosynthesis[20–22], or for pursuing applications in on-chip photochemistry, embedded biomedical sensors, optical computing, communications, and frequency standards[13]. To this end, plasmonic structures[23–33] and whispering gallery mode (WGM) resonators[6–13,34–49] provide optical elements for nascent systems but, considered separately, each presents significant limitations. Although effective as nanoantennas for both lasers and fluorescent optical sources[24,27,29–32,50–52], plasmonic sources are typically of low Q as a result of dissipative losses. Nevertheless, enhancements in the local electric field strength of orders of magnitude are available with plasmonic nanostructures in the form of (for example) bowties, spheres, cylinders, or cones, an attribute that is responsible for the detection of single nanoparticles and molecules by Raman scattering[53]. In contrast, as noted in reference 54, "… the electromagnetic field enhancement provided by WGMs is relatively weak when compared to that of plasmonic antennas …" but WGM resonators do offer Q values beyond $10^{11}$ (Ref. 40), thereby opening the door to microlasers in which the resonator is fashioned from the gain medium itself[6–9,34]. The long optical storage times implied by the values of Q available with WGM resonators (e.g., photon lifetimes, $\tau_p$, of 2 μs at $5 \times 10^{14}$ Hz when Q = $10^9$) enable weak nonlinear optical processes to be observed readily at field intensities several orders of magnitude lower than that required by the bulk nonlinear medium[35,38,41–43,55]. Pump thresholds of only a few photons per whispering gallery mode have been observed, and Raman gain coefficients for the nonlinear WGM resonator are increased by two orders of magnitude relative to bulk values[35]. The disparate, but synergistic, properties of plasmonic structures and WGM resonators suggest joining the two elements to form hybrid optoplasmonic systems[54,56–62]. Indeed, experiments of the past 7 years have demonstrated vividly that coupling plasmonic and photonic devices is effective in significantly improving the sensitivity of the Raman detection of molecules, or in transferring optical energy over distances of as much as several hundred nm[42]. Ahn et al.[54] have, for example, recently employed plasmonic nanoantennas to deliver optical radiation, by free-space transmission, to a spherical resonator with a coupling efficiency of 44%. Aligned with the equatorial plane of the microsphere, the nanoantennas were separated from the sphere surface by a mean distance of ~100–150 nm and each antenna radiated into the evanescent optical field of the resonator. Despite these advances, the functionality of existing hybrid optoplasmonic systems has been limited and, in particular, the integration of a narrow linewidth optical emitter with a broadband amplifier has not been demonstrated previously.

Expected to be the forerunner of a new class of compound optoplasmonic devices, the optically-pumped photonic/plasmonic amplifier described here is injection-seeded by the narrow bandwidth radiation provided by Raman scattering (1st Stokes) of the pump by the resonator medium (polystyrene) or, if desired, another component of the amplifier (protein tether, substrate, etc.). Injecting a seed signal into the amplifier effectively decouples the system Q from the resonator. That is, the amplifier Q is no longer constrained by the WGM resonator but rather can be dictated by the pump laser linewidth and the Raman mode providing the seed radiation. As opposed to having the gain medium in direct contact with[47], or at the perimeter of[63], the resonator, suspending the dye molecules above the resonator surface increases both the effective lifetime of the excited singlet state and, therefore, the energy stored by the medium. Furthermore, tethering the dye to the resonator ensures that the *entire* gain medium lies well within the evanescent field associated with power circulating in the microresonator. This nano/micro-optical system behaves in a manner similar to that of macroscopic master oscillator-power amplifiers (MOPAs), and the results presented later appear to represent the first report of the extraction of optical power from a gain medium, surrounding a WGM resonator, by a narrow band injection seed.

Figure 1a is a generalized diagram (not to scale) of the compound optoplasmonic amplifier. Dye molecules conjugated with a protein (NeutrAvidin: NA) are coated onto biotinylated polystyrene microspheres having a diameter, $d$, of nominally 2 μm or 10.1 μm. Tethering of the dye to the surface of the sphere with the biotin-avidin protein positions the molecules 11.1 ± 0.1 nm from the surface, thereby situating the dye well within the evanescent field of the WGMs associated with power circulating within the spherical microresonator. For the sake of clarity, only a single dye molecule is illustrated in Fig. 1a – the areal density of the molecules on the surface of the sphere will be discussed later. A single sphere is then placed onto the surface of a non-patterned (irregular) plasmonic array structure[64] comprising an 80 nm thick silver film deposited onto an aperiodic array of Si nanocones (see Supplementary Fig. S1). Facilitating the introduction of optical power into, and extraction of power from the microresonator, the plasmonic array constitutes an ensemble of nanoantennas[51,52,54] that serves as the equivalent of the output coupler common to macroscopic lasers. Although the Ag nanoglobules resting atop the nanocones have a distribution of geometries (spherical, ellipsoidal, clusters), the representative structure is taken to be that of ellipsoids having major and minor axes of 100 nm and 80 nm, respectively, in length. Also, small Ag spheres (typically 30 nm in diameter) lie between adjacent nanocones. A scanning electron micrograph (SEM) in plan view of a 2 μm diameter polystyrene sphere lying on the Ag-coated nanocone tips of a plasmonic array can be seen in panel d of Fig. S1 in the Supplementary Material. Illumination for the structure of Fig. 1a with CW laser radiation (He-Ne; λ = 632.8 nm or Nd:YAG (second harmonic); λ = 532 nm) is provided by a photoluminescence (PL) microscope having a numerical aperture of 0.45 and equipped with a 50× objective (Fig. S2). Measured by a scanning knife-edge technique (Fig. S6 of the Supplementary Material), the full width of the He-Ne laser beam at the surface of a microsphere is 1.1 μm. A laser power of 100 μW incident on a microresonator corresponds to an optical intensity at the sphere surface of 8 kW-cm$^{-2}$.

The WGMs available with the spherical microresonator of Fig. 1a were calculated by a vectorial, finite element method[65], and Fig. 1b shows the calculated dependence of the eigenmode resonance wavelength on the azimuthal mode number ($m$) for microspheres having diameters of 2, 10.1, and 15 μm. Note that the free spectral range (FSR) for the three microresonators in the λ ~ 650 nm region is
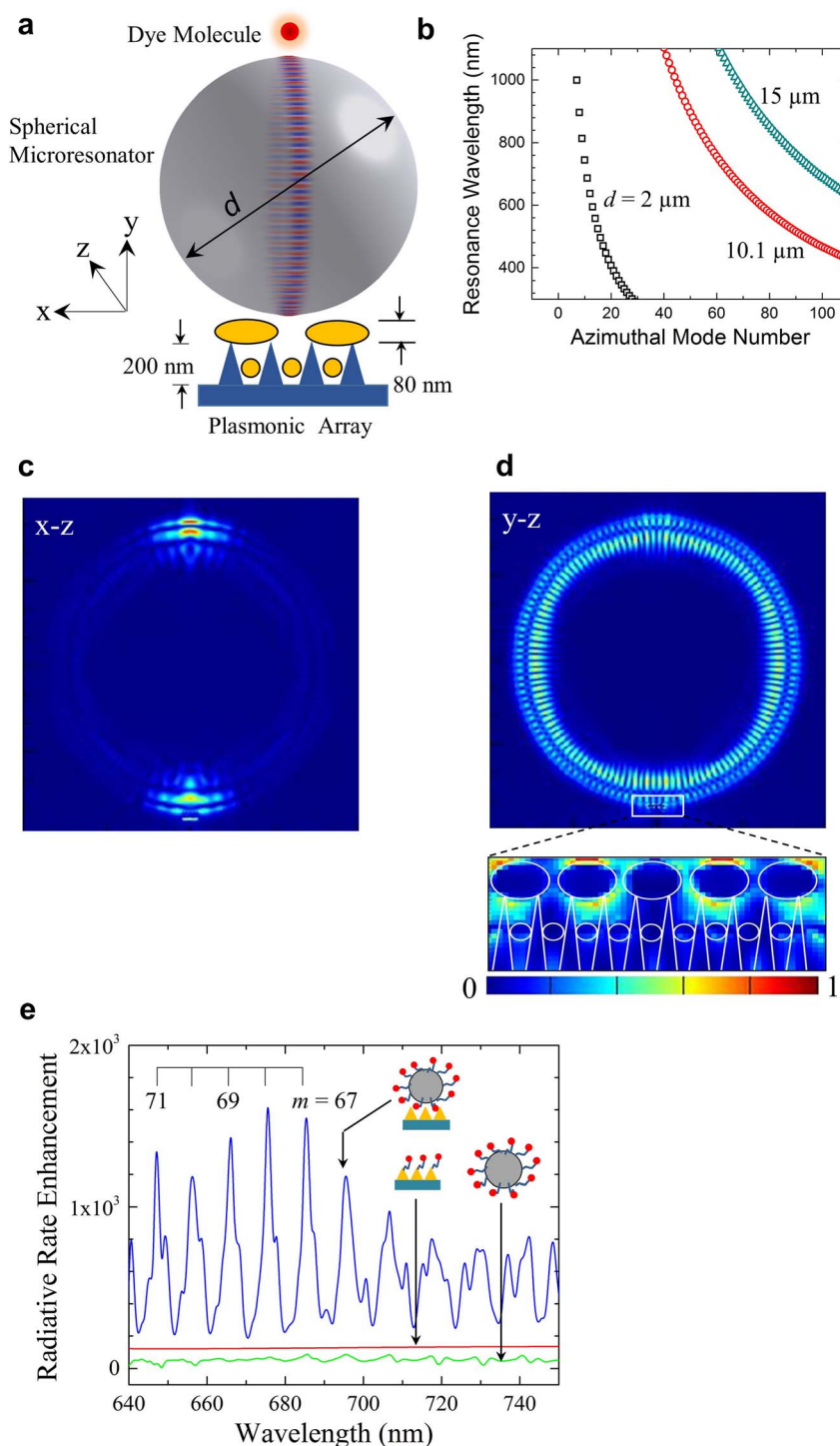
Figure 1 | Structure, design, and numerical simulations for the injection-seeded nano/micro-optical amplifier system. (a) Diagram (not to scale) of the optical amplifier, comprising a spherical whispering gallery mode resonator of diameter, $d$, dye molecules (one shown for the sake of clarity) tethered to the resonator surface, and a plasmonic array. The latter consists of silicon pillars or cones, 200 nm in height, onto which Ag is deposited. Metal ellipsoids resting on the cones have a minor axis of nominally 80 nm and an end-to-end separation of 20 nm. Small (~30 nm dia.) metal spheres are also produced between the cones. For the polystyrene spheres that served as resonators, $d$ was 10.1 μm or 2 μm and the index of refraction is 1.58; (b) Cavity mode dispersion curves calculated for polystyrene sphere diameters of $d$ = 2, 10.1, and 15 μm; (c) Calculated electric field intensity ($|\vec{E}|^2$) map for $d$ = 10.1 μm and λ = 676 nm ($m$ = 68), viewed along the $y$-axis (Fig. 1a); (d) Intensity distribution of c but viewed along the axis ($x$) orthogonal to the $y$–$z$ plane in which the WGM field intensity is maximum. A magnified portion of the field intensity extending into the plasmonic array is also shown, and the white lines outline the plasmonic array structure; (e) Comparison of the calculated enhancement of the dye molecule radiative rate, relative to the free space value, for the complete amplifier structure (blue), dye molecules tethered to the sphere (green), and dye molecules positioned 30 nm above the plasmonic array (red).
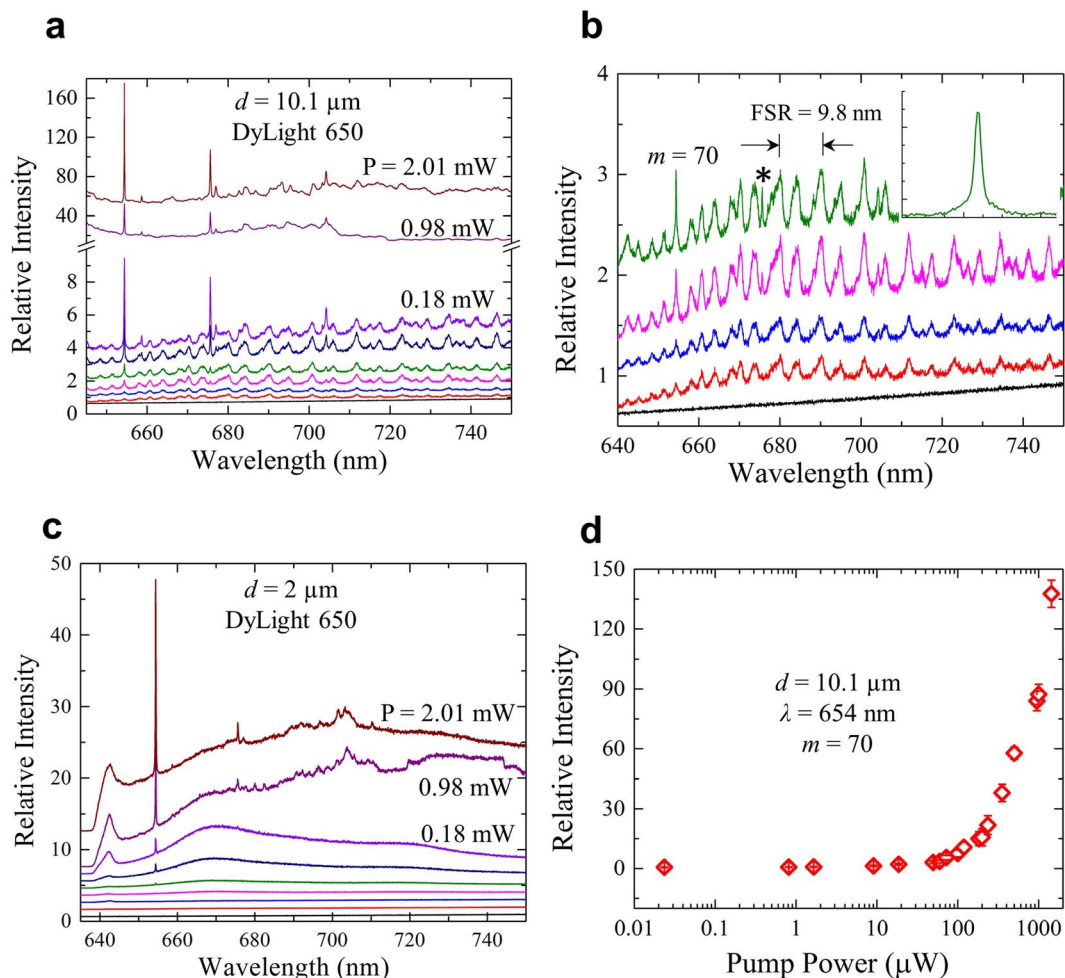
**Figure 2 | Injection seeding of optoplasmonic amplifiers with $d = 10.1$ µm or 2 µm WGM resonators.** (a) Photoluminescence (PL) spectra in the 650–750 nm region for an amplifier incorporating a $d = 10.1$ µm resonator to which Dylight 650 dye is conjugated. Nine spectral scans, recorded for $\lambda = 632.8$ nm pump powers ranging from 24 nW to 2.0 mW, are given, and for clarity, are displaced vertically from one another. Note the change in the scale of the ordinate for the two uppermost spectra; (b) Magnified view of the five lowest-power spectra from a). Note the emergence of the amplified Raman (1st Stokes) line at 654 nm and a weaker feature at 676 nm (denoted by an asterisk). The inset provides a view of the m = 70 WG mode, and the superimposed, amplified Raman signal, at higher magnification; (c) Spectra similar to those of panel a) but acquired with a $d = 2$ µm microresonator and Dylight 650 dye attached to the resonator. The selective amplification of the 654 nm Raman line is evident, and the laser excitation powers ($\lambda = 632.8$ nm) again range from 24 nW to 2 mW. The broad continua at ~642 nm and the structure near 702 nm are due to the Ag nanolayer; (d) Variation of the relative intensity of the 654 nm output with the 632.8 nm excitation power for a $d = 10$ µm microresonator.

42.6 nm, 9.5 nm, and 6.3 nm for $d = 2$, 10.1, and 15 µm, respectively. Panels c and d of Fig. 1 are color-coded images illustrating the squared magnitude of the local electric field ($|\vec{E}|^2$), calculated by a finite-difference time domain (FDTD) algorithm for a spherical microresonator and assuming $d$ and $m$ to be 10.1 µm and 68 ($\lambda \sim 676$ nm), respectively. As described in detail in the *Methods* section, these calculations were based on a single dipole (molecule) situated 100 nm from the polystyrene microsphere surface, and the dipole polarization is oriented along the $y$ axis of Fig. 1a. In Fig. 1d, the mode pattern is viewed along an axis ($x$) orthogonal to the $y$–$z$ plane in which the spatially-averaged mode intensity is maximum. Observing the same intensity distribution in the $x$–$z$ plane itself results in the map of Fig. 1c. A magnified view of the field intensity extending from the microresonator into the underlying plasmonic array structure (cf. Fig. 1a) is given by the inset to Fig. 1d. As expected, the electric field strength is greatest at the spherical resonator/plasmonic surface interface and the region between the silver-coated nanocones. Similar results for the $d = 2$ µm microresonator can be found in the Supplementary Information (Figs. S7–S9). Calculations of the enhancement of the dye radiative rate, relative to that for the dye

on a flat surface, are summarized in Fig. 1e for various combinations of the three components of the amplifier. As discussed in Sect. 9 of the Supplementary Information, the enhancement in the dipole (dye) radiative rate is calculated by determining the time-integrated power outflow from the optical structure under consideration. Ignoring for the moment the influence of an optical signal injected into the microresonator, the full optoplasmonic amplifier (dye, spherical resonator, and plasmonic array- blue curve) yields calculated radiative rates three orders of magnitude larger than those for the dye alone. Peak enhancements are observed at the WGM resonance wavelengths, and the spectral widths (FWHM) of 2 nm for the m = 69–72 modes indicate that the expected value of Q for the microresonator alone is at least 300. It will be demonstrated later that this estimate is in agreement with experimental spectra. As illustrated by the green trace of Fig. 1e, the enhancement of the dye radiation rate falls precipitously when the plasmonic array is removed from the amplifier (leaving only dye molecules tethered to the microsphere resonator). Similarly, if the resonator is removed and the dye is positioned 30 nm above the surface of the plasmonic array, peak enhancements of ~80 in the radiative rate are observed (red curve,

Fig. 1e - the red and green curves are separated vertically for clarity). It must be emphasized that the relative contributions of the resonator and plasmonic array to the overall dye emission intensity are of secondary importance, since different design parameters ($d$, plasmonic array structure) are capable of reversing the relative magnitudes of their respective enhancements. Rather, as illustrated by Fig. 1e, the critical point to be made is that the combined action of the three amplifier components produces radiative enhancements 2-3 orders of magnitude larger than those offered by the plasmonic array or the resonator alone.

Irradiating the optoplasmonic structure of Fig. 1a with the focussed beam of a CW He-Ne laser (632.8 nm) results in the photoluminescence spectra of Fig. 2a. Data are presented for nine values of laser power (P), ranging from 24 nW to 2.0 mW, and with DyLight 650 dye (MW = 1357) tethered to a 10.1 μm diameter polystyrene sphere by biotin-NA. For the lower values of excitation power (P < 1 mW), the WGM structure is clearly present but spectrally-narrow features are also observed, the most intense of which lie at 654.3 and 675.7 nm. Indeed, as the laser excitation power is increased, the undulations due to the WGMs diminish in intensity and the spectra are dominated by these two narrow lines. Measurements of the linewidths of these features show them to be below the instrument (spectrometer) spectral resolution of $5 \times 10^{-3}$ nm. Magnifying the five spectra of Fig. 2a that were recorded at the lowest laser power levels reveals that the line at 654.3 nm lies atop the peak of the $m = 70$ mode of the 10.1 μm diameter sphere, and is considerably narrower than the mode profile. The inset to Fig. 2b provides a further expanded view of the $m = 70$ WGM and the superimposed, narrow line. In contrast to the emission at 654 nm, the 675.7 nm feature (identified by the asterisk in Fig. 2b) lies between two WGM maxima. Note, too, that the observed FSR for the microresonator (9.8 nm at 680 nm) is in agreement with the calculated value (Fig. 1b) of 9.5 nm for $\lambda = 650$ nm. When the microsphere diameter is reduced to 2 μm, the dominance of one (or a few) intense features is more dramatic than that observed for the larger resonator. As illustrated by the spectra of Fig. 1c which were acquired with the dye DyLight 650 attached to the polystyrene microsphere, the line at 654 nm dwarfs all of the discrete structures in the 638–750 nm spectral region. Spectra presented in the Supplementary Material (Fig. S10) demonstrate that the continuum at $\lambda \sim 642$ nm and the structure in the vicinity of 702 nm arise from the Ag nanolayer. Measurements of the variation of the relative intensity at 654 nm with the laser excitation power, summarized in Fig. 2d, show a rapid rise in the detected signal (at $\lambda = 654$ nm) for a 10.1 μm diameter sphere and incident powers above 100 μW.

The origin of the narrow lines of Fig. 2a–c becomes apparent in Fig. 3 where the output spectrum for the optoplasmonic amplifier is compared with the Raman spectra recorded for the microsphere resonator and (separately) biotin-avidin. In this figure, wavelength is expressed on the lower abscissa in terms of the red-shift with respect to the laser excitation frequency ($\lambda = 632.8$ nm, $\tilde{v} = 15{,}798.02$ cm$^{-1}$). For convenience, FDTD calculations of the WGM spectrum for a $d = 10.1$ μm polystyrene sphere in the 655–720 nm region are also given (please refer to Fig. S5 of the Supplementary Information). Of the most intense features observed in Fig. 2 - 654.3, 675.7, and 704.2 nm – the latter two are matched precisely by the strongest Raman lines (1$^{st}$ Stokes) of polystyrene. The dominant Raman mode in the polystyrene spectrum at 1002 cm$^{-1}$ (Fig. 3b) was first reported by Cornell and Koenig[66] in 1968. One concludes that the prominence of the polystyrene Raman lines in the amplifier output spectrum is the result of two factors, the first of which is that the generation of Raman radiation at 1002 cm$^{-1}$ and 1602.7 cm$^{-1}$ occurs throughout the sphere and the scattered radiation is largely confined to the sphere by internal reflection, owing to the polystyrene refractive index of 1.58. The second consideration is that the fluorescence spectrum for the dye tethered to the sphere
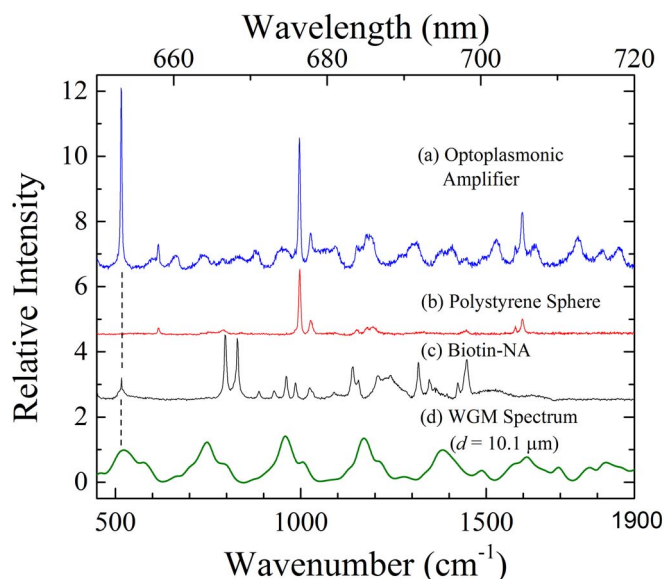


**Figure 3 | Comparison of Raman and whispering gallery mode spectra for the injection-seeded amplifier.** (a) Output spectrum of the amplifier for 182 μW of laser excitation power at 632.8 nm; (b) Raman spectrum between 500 cm$^{-1}$ and 1900 cm$^{-1}$ for the microresonator alone (polystyrene sphere); (c) Raman spectrum for the Biotin-NA complex over the same spectral range; (d) WGM spectrum (TE modes) for a $d = 10.1$ μm sphere, calculated by a FDTD procedure. The dashed vertical line illustrates the coincidence of the 520 cm$^{-1}$ Raman mode with a local maximum (resonance) in the WGM spectrum.

(Dylight 650) peaks at ~680 nm (Fig. S5 of the Supplementary Material), and maximum optical gain is expected to occur in the 680–690 nm interval (red-shifted from peak fluorescence by absorptive losses). Consequently, the polystyrene Raman lines are amplified by the dye as the evanescent field associated with optical power circulating in the microsphere extracts energy from the dye molecules that are optically-excited by the incident laser radiation. We also point out that gain profiles for dyes such as Dylight 650 are known to be homogeneously-broadened and, therefore, injection-seeding of the gain profile with a narrow- band input signal (such as that provided by Raman scattering) will result in the efficient extraction, by that narrow band "seed", of energy stored in the electronic excited states of the dye[15,18].

The role of the dye in the amplification of the 1002 cm$^{-1}$ and 1602.7 cm$^{-1}$ Raman mode emission of polystyrene is confirmed by experiments in which the radiative output of the amplifier is monitored with and without dye tethered to the microresonator. Figure 4a summarizes measurements of the relative intensity of the 675.7 nm Raman line for several values of the laser excitation power. Results are given for the full amplifier structure (denoted by the shaded square symbols), and various combinations of the microsphere, dye, and plasmonic array. Removing the dye from the microresonator results in a greater than one order of magnitude drop in the output intensity at this wavelength. One concludes, therefore, that the mechanism responsible for the observed amplification is injection-seeding of the dye gain profile, a process quite distinct from those giving rise to Raman scattering enhancements in microdroplets[35], Raman lasers in microspheres[43], and Raman-injected quantum cascade lasers[67]. It is the combined action of all three elements of the amplifier of Fig. 1a (nanostructured array, WGM resonator, and the gain medium) that distinguishes this amplifier from the nano/micro optical devices that precede it. Before discussing other aspects of the spectra of Fig. 2a–c, it should be noted that, at the highest laser pump powers available for these experiments, degradation of the dye gain medium was observed. Nevertheless,
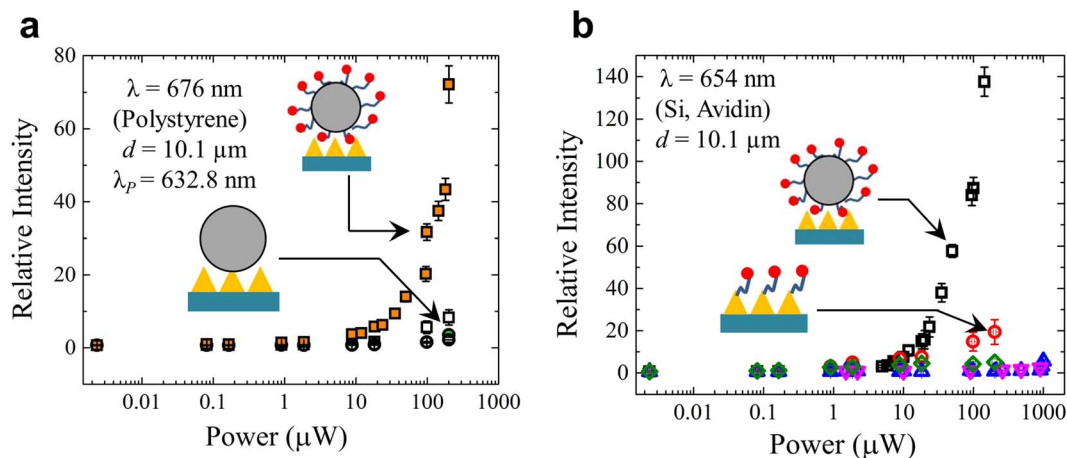
Figure 4 | (a) Amplification of Raman seed radiation at 675.7 nm ($\lambda_{pump}$ = 632.8 nm; Raman mode of polystyrene at 1002 cm$^{-1}$) with the full dye/resonator/plasmonic array system ( ■ ) and various combinations of the three components. The open squares ( □ ) represent data obtained with the plasmonic surface and the microresonator but with the dye removed from the resonator surface. All error bars represent uncertainties of ±1σ in the measurements. The circular data points denote data obtained with the microresonator with dye ( ● ), and the microresonator alone ( ○ ); (b) Data similar to those of panel a) but obtained for the $\lambda$ = 654 nm Raman line of Biotin (or Si). Results associated with the dye alone, dye tethered to the microsphere, and the microsphere (without dye) on the plasmonic array are represented by the diamond ( ◇ ), triangular ( Δ ), and inverted triangular ( ▽ ) symbols, respectively. Error bars again denote an uncertainty of one standard deviation.

short exposures of the amplifier to the pump beam yield reliable spectra and several WGMs are clearly present even in the P = 2.0 mW spectrum of Fig. 2a. In the interest of caution, however, the discussion to follow will emphasize spectra acquired for pump powers below 1 mW.

Of perhaps greatest interest in the output spectrum of Fig. 3a is the dominant line at 520 cm$^{-1}$ that coincides with a weak feature in the Biotin-NA spectrum. Well known from Raman spectroscopy of the biotin-avidin complex with both laser and incoherent sources[68], this frequency is associated with the S–S stretching mode for the sole disulfide unit in avidin[69]. As indicated by the dashed vertical line in Fig. 3, the position of the 520 cm$^{-1}$ Raman mode of Biotin-NA also matches closely (for a driving wavelength of 632.8 nm) the peak of the $m$ = 70 WGM profile. Virtually all of the other biotin-avidin Raman features fall between WGM resonances. An alternative assignment for the 654.3 nm feature of Figs. 2a and 2c is the well-known 521 cm$^{-1}$ Raman mode of Si. Although the nanostructured Si substrate is covered by an Ag nanolayer, weak Raman scattering is observed from the overcoated Si substrate at 654.3 nm when the laser excitation power is at its highest level. Supplementary Fig. S10 shows the faint emission observed from an Ag/Si nanocone substrate alone. The close coincidence between the frequencies of the avidin and Si Raman modes, in combination with the wavelength calibration process and the dispersion of the spectrograph available for these experiments, precludes a definitive identification of the 654.3 nm line of Figs. 2 and 3. Regardless of the source, however, the seed emission is quite weak and the match between the injected Raman signal and the peak of the $m$ = 70 whispering gallery mode leads one to expect the microresonator to have the greatest impact on the amplifier output at the wavelength of 654.3 nm. This presumption is borne out by the lower half of Fig. 4 which compares the relative intensity of the 654.3 nm output signal recorded for the full amplifier (denoted by the open square symbols) with that produced by other component combinations. In particular, removing the microresonator and attaching the dye directly to the plasmonic surface (represented by the red open circles of Fig. 4b) again reduces the amplifier output intensity by more than an order of magnitude when the laser excitation (pump) power is 100 µW. Consequently, the plasmonic contribution to the overall output intensity of the amplifier is greater in this case than that of the resonator (i.e., the resonator and dye alone in Fig. 4b yield comparatively low output), but neither the nanoplas-

monic array nor the microresonator separately (although coupled to the gain medium) approach the performance of the full amplifier.

On the basis of Figs. 2a and 2c, as well as other spectra not presented, it is clear that the rate of growth of the 654.3 nm line ($\sim$520 cm$^{-1}$ Raman mode) intensity outpaces that for the polystyrene lines that do not lie on a WGM peak. We conclude, therefore, that the coincidence of a particular Raman mode of avidin (or Si) with a specific WGM of the spherical resonator results in the amplification of the seed radiation at this frequency, to the exclusion of other Raman lines and microresonator modes. Furthermore, the near collapse of the WGM structure in Fig. 2a as the pump power is increased is consistent with the behavior of all injection-seeded amplifiers[15,19]. Specifically, a signal injected into the amplifier will extract energy stored under the gain profile, provided that the gain medium is homogeneously-broadened (which is known to be the case for the dyes employed here) and the injection seed wavelength is matched to the dye gain spectrum. It is not surprising, therefore, that the WGM structure does not intensify at the higher pump powers. On the contrary, the WGM spectrum diminishes quickly in intensity with increasing pump power, and the broadband fluorescence characteristic of the dye is not observed- the seed appears to be extracting optical power that is emitted elsewhere in the spectrum when the pump intensity is lower.

Results similar to those of Figs. 2 and 4 were obtained when a green dye (Cy-3) was substituted for Dylight 650 and the amplifier was irradiated with the second harmonic of the Nd:YAG laser ($\lambda$ = 532 nm). A portion of the data obtained in these experiments is presented in Fig. 5 which compares the relative amplifier output intensity for Cy-3 dye with that for another red dye (Cy-5) as the excitation intensity is varied. When the amplifier is irradiated at 532 nm, the 1002 cm$^{-1}$ Raman line of polystyrene lies at 563 nm and strong amplification is observed in Fig. 5 for the Cy-3 dye, presumably because the Raman line of interest coincides with the peak of the dye gain profile ($\lambda$ = 560 nm). However, substituting the red dye Cy-5 for Cy-3 in these experiments yields a null result, thus affirming the requirement that operation of the amplifier and realizing maximum amplification, in particular, is dependent upon matching the wavelength of the internally-generated Raman signal with the gain spectrum of the dye. We also point out that the demonstration of the amplification process, reported here in two regions of the visible, confirms the versatility of the design.

Before proceeding, several comments regarding the Q of the amplifier and the contribution of the Ag nanolayer to amplifier performance are warranted. Spectra similar to those of Fig. 2, but recorded with amplifiers from which the Ag plasmonic layer has been removed, confirm the expected degradation of Q that results from the dissipative losses introduced by the metal. Supplementary Fig. S11 compares output spectra in the 670–690 nm region that are produced by an amplifier when the Ag nanolayer is present, or has been removed. Analysis of Fig. S11 and similar spectra finds that the amplifier Q is decreased by a factor of ~5 when the metal nanolayer is inserted. For the full structure of Fig. 1a, the amplifier Q is calculated to be $357 \pm 25$ (if the impact of the injection signal is ignored for the moment), a value in agreement with the FDTD calculations mentioned earlier. When the Ag layer is removed, however, the amplifier Q rises to $1523 \pm 50$. Although the Q of the amplifier falls with the introduction of the Ag nanolayer on the Si substrate, the presence of Ag strengthens significantly the emission spectrum of the amplifier and particularly in the 690–750 nm region. Integrating over the entire spectrum (cf. Fig. 2), for example, shows the photon fluence (e.g., wavelength-integrated intensity) to rise by more than 50% when the Ag nanolayer is included in the amplifier structure, and the pump power is only 18.6 µW (cf. Fig. S11). When the incident optical power is increased to 2.01 mW, the enhancement in integrated output fluence rises to 1280. Therefore, it is clear that the Ag nanolayer plays a plasmonic role in the operation of the amplifier, as evidenced by the enhancement of its radiative output. Of greater significance is the fact that the *effective* Q of the optical amplifier reported here is not constrained by the Q of the resonator itself. Unlike previous WGM resonator-based devices, the system Q can be determined by the spectral breadth of the Raman signal which, in turn, is often limited by the linewidth of the pump radiation. In Fig. 2b, for example, the Raman signal is considerably narrower than the spectral profile for the $m = 70$ azimuthal mode of the resonator. Although the spectral width of the amplified Raman signal cannot be measured precisely at present, a lower bound for the effective Q of the amplifier at 654.3 nm is $10^5$.

Further evidence supporting the contention that the structure of Fig. 1a is an optical amplifier is provided by experiments in which the dye is repositioned with respect to the microresonator and the plasmonic surface. Consider, for example, the spectrum of Fig. 6 indicated by the black trace that was recorded with the dye/plasmonic
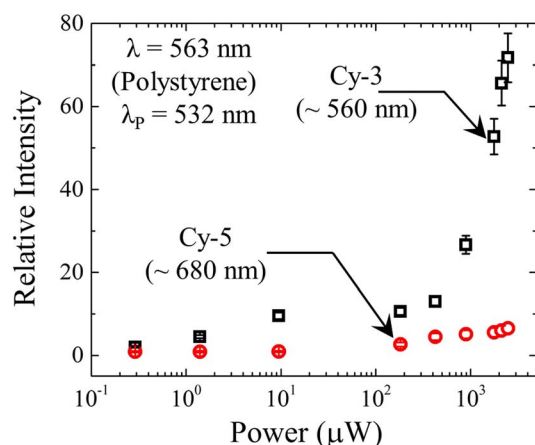
array/resonator arrangement shown schematically by the inset. When the dye is no longer tethered to the resonator surface but rather is attached to the plasmonic surface and, thus, is situated between the microresonator and plasmonic array, the Raman lines of Figs. 2 and 3 vanish, irrespective of the pump power (measured over the range in pump power of P = 2.9 µW to 1.8 mW). Superimposed onto an intense broad continuum that is characteristic of the fluorescence profile of the dye (Cy-5, in this case), the structured portion of the spectrum is no longer a signature of the resonator material (polystyrene) but rather is also generated by the dye. Similarly, the WGMs associated with the microresonator are no longer observed. Additional data (presented in Fig. S14 of the Supplementary Information) demonstrate that, as the excitation power is increased, no feature in the discrete spectrum of Fig. 6 (black curve) intensifies significantly at the expense of the others, and the relative strength of all of the narrow features remains constant. Perhaps most significantly, virtually all of the power of Fig. 6 is radiated spontaneously and the background continuum is not suppressed (indeed, the underlying continuum is dominant). All of these observations indicate that the discrete portion of the spectra of Fig. 6 represents surface-enhanced Raman scattering (SERS) of the dye itself[39], a conclusion confirmed by the red trace of Fig. 6. The data of Fig. 6 show clearly that situating the dye between the microsphere and the plasmonic surface decouples the gain medium from the resonator, and the synergistic interaction of the dye, resonator, and plasmonic array in selectively amplifying specific Raman lines by channeling energy from the dye to the resonator, has been lost. In short, tethering the dye directly to the nanoplasmonic surface (inset to Fig. 6) yields an arrangement similar to that of SERS experiments of the past decade[39,41,42]. Removing the dye from the microresonator surface and placing it at the interface between the sphere and nanoplasmonic array alters dramatically the function of the system. No longer are the WGMs of the spherical microresonator amplified, and Raman emission produced within the resonator is not detectable. Understandably, therefore, only the SERS spectrum for the dye (also see Fig. S15 and Table S1 of the Supplementary Information), and its characteristic emission continuum, are observed. Both are absent when the amplifier is functioning properly.

Determining the gain of the optical amplifier is challenging because the input signal to the amplifier is the weak Raman emission generated internally to the amplifier. However, an estimate can be obtained by normalizing the visible emission intensity produced by the full structure (for a specific pump power) to that generated by the
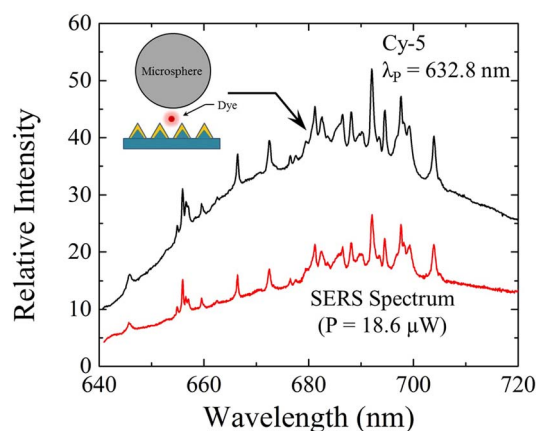


**Figure 5** | **Photoexcitation data similar to those of Fig. 4, illustrating the requirement for an overlap of the dye gain spectrum with a Raman line of interest.** In obtaining these data, the laser excitation wavelength was 532 nm and the relative intensity of the polystyrene Raman line at 563 nm was recorded. Results are shown for both green (Cy-3) and red (Cy-5) dyes. Error bars again represent an uncertainty of one standard deviation in the measurements.



**Figure 6** | (Top) Photoluminescence spectrum recorded when Cy-5 dye is no longer tethered to the spherical resonator but rather is repositioned as shown by the inset diagram; (Bottom) Raman (SERS) spectrum for Cy-5 alone on the Ag/Si plasmonic surface: These spectra were acquired with a 50× objective, an accumulation (integration) time of 10 s, and a $d = 10.1$ µm resonator.

equivalent number of dye molecules in solution. Because the biotin-avidin complex has a hydrodynamic diameter of $11.1 \pm 0.1$ nm[70] and an average of 1.9 dye molecules bind to each complex, then the mean number of molecules that are tethered to a 10.1 μm diameter microsphere is $1.6 \times 10^6$ at saturation. Consequently, only 4750 molecules are calculated to lie within the 1.25 μm$^2$ spot size of the pump laser beam at the microsphere surface. Almost precisely the same number of dye molecules exists in 1 μL of a 100 nM dye solution. Comparisons of the visible emission intensity produced by the optical amplifier with that generated by the dye solution applied to a glass surface showed (for a fixed value of laser excitation power) the amplifier emission to be a factor of $1280 \pm 30$ larger than that from the dye alone. Therefore, one estimate for the gain of the amplifier is ~30 dB. This simple estimate is expected, however, to provide only an upper limit because the calculation ignores the dye molecules, surrounding the sphere, that are optically excited by the portion of the pump radiation that is transmitted initially by the sphere but is scattered back into the resonator by the Ag/Si nanoarray.

A final measurement that should be mentioned is the observation of the effective lifetime of the dye molecules in the amplifier. Because the biotin-avidin tether displaces these emitter molecules ~11 nm from the surface of the sphere, the effective lifetime of Cy-3 molecules (for example) is expected to be increased. Indeed, frequency-domain lifetime imaging microscopy (FLIM)[71] measurements determined the Cy-3 dye excited state lifetime to be 1.5 ns, or approximately twice that for the same dye in solution. As mentioned earlier, therefore, suspending the gain medium above the resonator surface minimizes non-radiative quenching of the electronically-excited species. Details concerning these measurements can be found in the Supplementary Material at Fig. S13.

In summary, a nano/micro-optical amplifier in the visible has been demonstrated in which specific Raman lines, generated internally to a spherical microresonator (or by another component of the amplifier) are amplified in an injection-seeding process that extracts power from the gain medium surrounding the resonator. The evanescent portion of the optical field circulating in the microresonator harvests energy from optically-excited dye molecules, all of which are held in close proximity to the resonator surface by a protein tether. An aperiodic nanoplasmonic array in physical contact with the microresonator serves to couple optical power out of, and into, the system but also to enhance the local electric field strength in the resonator, thereby accelerating the growth rate of the Raman signal and increasing the total optical power emitted by the amplifier. In this optoplasmonic amplifier (shown schematically in Fig. 7), the linewidth of the output radiation is determined primarily by the seed which, in turn, is specified by the Raman mode selected and the pump laser linewidth. Consequently, the effective Q of the amplifier is not limited by the microresonator. Amplification of only specific Raman lines is achieved by matching a resonator WGM, and the gain profile of the dye, with the frequency of the Raman line of interest. Consequently, the synergistic effect of the microsphere, the nanoplasmonic surface, and the gain medium is considerably greater than that of any component alone (or any set of two). Demonstrating this amplifier concept with a weak Raman mode of the biotin-avidin tether or the Si substrate illustrates the potential of the approach for realizing optical devices suitable for generating, amplifying, and routing optical energy at the microscale. Furthermore, replacing dye with other gain media, such as rare earth-doped nanocrystals having atomic transitions with upper state lifetimes considerably larger than those for the excited singlet states of dyes (a few ns), will improve significantly the energy storage capabilities of the amplifier. Specifically, optimal energy storage in, and output power of, this amplifier is expected when the photon lifetime $\tau_p \equiv Q/\omega$ of the optical resonator is matched to the excited state lifetime for the gain medium. It should also be mentioned that the structure and emission characteristics of this amplifier suggest the feasibility of embedding
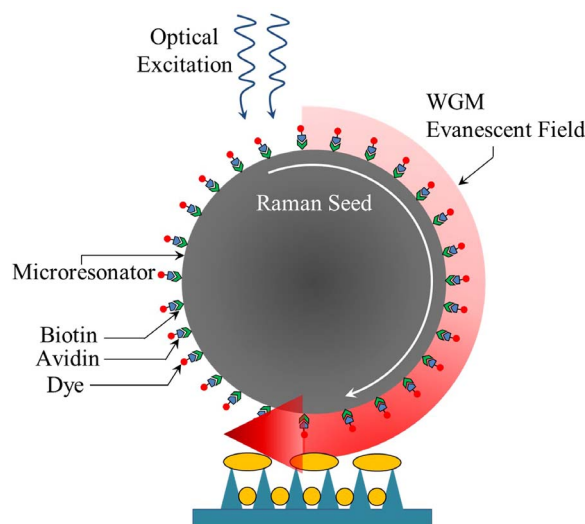


**Figure 7** | **Cross-sectional diagram of the hybrid optical/plasmonic amplifier (not to scale), illustrating the primary processes responsible for its behavior.** For clarity, the plasmonic array has been separated from the microresonator.

one or more within tissue or another highly-scattering biological or inorganic medium. Capable of being photopumped from outside the medium in which it is buried, this amplifier (or arrays of amplifiers) can serve as an *in situ* diagnostic of biological or chemical activity.

## Methods

**Fabrication of plasmonic array.** Photolithography and a reactive ion etching process are used to fabricate the plasmonic substrate on a 4-inch (10 cm) diameter wafer. First, the area where nanocone structures are to be etched is patterned by photolithography. Secondly, in a mixture of HBr and O$_2$ gases, the silicon substrate is etched by HBr and oxidized by O$_2$ simultaneously. The nanocone structures are synthesized by taking advantage of the high etching selectivity of HBr for silicon, relative to its oxide (200: 1). Finally, a thin (80 nm) silver coating is evaporated onto the Si nanocone array.

**Conjugation protocol: Attaching dye to the microspheres.** The biotinylated polystyrene microspheres (MS) are obtained from Bangs Laboratories Inc. and dye (NeutrAvidin Dylight 650 (NA-Dy), 1 mg/mL) was purchased from Thermo Scientific. Five hundred microliters of NA-Dy solution (100 μg/mL) was prepared with PBS buffer and 50 μL of microspheres in storage buffer (100 mM Borate, pH 8.5 + 0.01% BSA +0.05% Tween® 20 + 10 mM EDTA + ≤0.1% NaN$_3$) was mixed with the NA-Dy solution in a 1 : 10 ratio. The mixture was incubated on a shaker for 30 minutes (or 0.5–2 hrs, depending on the concentration) and covered by aluminum foil. Subsequently, the solution was centrifuged at 3000 rpm for 2 min and re-suspended with the buffer using a vortex mixer. The procedure was repeated 4 times. Finally, a 1 μL drop from the solution was cast onto the glass/plasmonic substrate for further experimentation.

**Calculation of the number of dye molecules conjugated to microspheres.** The concentration of protein (NA) in the sample was measured with a NanoDrop ND-1000 spectrophotometer (Nano Drop Technologies, Rockland, Delaware, USA) by using the absorbance value at 280 and 650 nm ($A_{280}$ and $A_{650}$). The protein concentration was determined from the expression: Protein concentration, $M = [A_{280} - CF \times A_{650}] \times dilution factor/\varepsilon$, where $\varepsilon$ is the molar extinction coefficient of the protein, and *CF* is the correction factor for the dye's contribution to $A_{280}$. The degree of labeling, DOL, (moles of dye per mole of protein) was calculated as: $DOL = A_{650} \times dilution factor/(\varepsilon' \times protein concentration(M))$, where $\varepsilon'$ is the molar extinction coefficient for the fluorescent dye.

**Numerical simulations.** The whispering gallery modes inside the spherical microresonator were simulated by COMSOL. As the geometry of the resonator is axisymmetric, a two-dimensional representation model was employed. Oxborrow lists the system of differential equations for simulating whispering gallery modes[65] and, with COMSOL, a mesh was generated and the resonant frequency of the optical mode near the specified mode number was calculated. In order to determine the power enhancement produced by the amplifiers, a three dimensional finite-difference time-domain method was implemented with software from Lumerical Solutions, Inc. An electric dipole source was placed 100 nm above a 10.1 μm diameter polystyrene sphere. The polarization of the dipole was oriented along the y-axis of Fig. 1, and the emitter was assumed to emit a fluorescence spectrum peaking at 676 nm and having a

spectral width (FWHM) of 70 nm. For the sake of simplicity, the plasmonic array underlying the spherical resonator was assumed to be a periodic, 5 × 5 array of nanocones with a periodicity of 120 nm. The electric field distribution over the entire structure was calculated with a mesh size of 1 nm.

1.  Maiman, T. Stimulated optical radiation in ruby. *Nature* **187**, 493–494 (1960).
2.  Sorokin, P. & Stevenson, M. Stimulated infrared emission from trivalent uranium. *Phys. Rev. Lett.* **5**, 557–559 (1960).
3.  Gather, M. C. & Yun, S. H. Single-cell biological lasers. *Nature Photon.* **5**, 406–410 (2011).
4.  Arakawa, Y. & Sakaki, H. Multidimensional quantum well laser and temperature-dependence of its threshold current. *Appl. Phys. Lett.* **40**, 939–941 (1982).
5.  Duarte, F. & James, R. Tunable solid-state lasers incorporating dye-doped, polymer-nanoparticle gain media. *Opt. Lett.* **28**, 2088–2090 (2003).
6.  Tzeng, H. M., Wall, K. F., Long, M. B. & Chang, R. K. Laser-emission from individual droplets at wavelengths corresponding to morphology-dependent resonances. *Opt. Lett.* **9**, 499–501 (1984).
7.  Kuwata-Gonokami, M., Takeda, K., Yasuda, H. & Ema, K. Laser-emission from dye-doped polystyrene microsphere. *Japanese J. Appl. Phys. Part 2-Lett.* **31**, L99–L101 (1992).
8.  Sandoghdar, V. *et al.* Very low threshold whispering-gallery-mode microsphere laser. *Phys. Rev. A* **54**, R1777–R1780 (1996).
9.  Cai, M., Painter, O., Vahala, K. J. & Sercel, P. C. Fiber-coupled microsphere laser. *Opt. Lett.* **25**, 1430–1432 (2000).
10. Armani, D. K., Kippenberg, T. J., Spillane, S. M. & Vahala, K. J. Ultra-high-Q toroid microcavity on a chip. *Nature* **421**, 925–928 (2003).
11. Yang, L., Carmon, T., Min, B., Spillane, S. M. & Vahala, K. J. Erbium-doped and Raman microlasers on a silicon chip fabricated by the sol-gel process. *Appl. Phys. Lett.* **86**, 091114 (2005).
12. Grudinin, I. S., Matsko, A. B. & Maleki, L. Brillouin lasing with a CaF$_2$ whispering gallery mode resonator. *Phys. Rev. Lett.* **102**, 043902 (2009).
13. Hartnett, J. G., Locke, C. R., Ivanov, E. N., Tobar, M. E. & Stanwix, P. L. Cryogenic sapphire oscillator with exceptionally high long-term frequency stability. *Appl. Phys. Lett.* **89**, 203513 (2006).
14. Anger, P., Bharadwaj, P. & Novotny, L. Enhancement and quenching of single-molecule fluorescence. *Phys. Rev. Lett.* **96**, 113002 (2006).
15. Siegman, A. E. in 1129–1170 (University Science Books, 1986).
16. Goldhar, J. & Murray, J. R. Injection-locked, narrow-band KrF discharge laser using an unstable resonator cavity. *Opt. Lett.* **1**, 199–201 (1977).
17. Greene, D. P. & Eden, J. G. Injection locking and saturation intensity of a cadmium iodide laser. *Opt. Lett.* **10**, 59–61 (1985).
18. Farkas, A. M. & Eden, J. G. Pulsed dye amplification and frequency-doubling of single longitudinal mode semiconductor-lasers. *IEEE J. Quant. Electron.* **29**, 2923–2927 (1993).
19. Zheng, J. *et al.* Tunable ring laser with internal injection seeding and an optically-driven photonic crystal reflector. *Opt. Express* **20**, 14292–14301 (2012).
20. Pullerits, T. & Sundstrom, V. Photosynthetic light-harvesting pigment-protein complexes: Toward understanding how and why. *Acc. Chem. Res.* **29**, 381–389 (1996).
21. Collini, E. *et al.* Coherently wired light-harvesting in photosynthetic marine algae at ambient temperature. *Nature* **463**, 644–U69 (2010).
22. Hildner, R., Brinks, D., Nieder, J. B., Cogdell, R. J. & van Hulst, N. F. Quantum coherent energy transfer over varying pathways in single light-harvesting complexes. *Science* **340**, 1448–1451 (2013).
23. Oulton, R. F. *et al.* Plasmon lasers at deep subwavelength scale. *Nature* **461**, 629–632 (2009).
24. Suh, J. Y. *et al.* Plasmonic bowtie nanolaser arrays. *Nano Lett.* **12**, 5769–5774 (2012).
25. van Beijnum, F. *et al.* Surface plasmon lasing observed in metal hole arrays. *Phys. Rev. Lett.* **110**, 206802 (2013).
26. Stockman, M. I. The spaser as a nanoscale quantum generator and ultrafast amplifier. *J. Opt.* **12**, 024004 (2010).
27. Koenderink, A. F. On the use of Purcell factors for plasmon antennas. *Opt. Lett.* **35**, 4208–4210 (2010).
28. Sorger, V. J., Oulton, R. F., Yao, J., Bartal, G. & Zhang, X. Plasmonic Fabry-Perot nanocavity. *Nano Lett.* **9**, 3489–3493 (2009).
29. Kinkhabwala, A. *et al.* Large single-molecule fluorescence enhancements produced by a bowtie nanoantenna. *Nature Photon.* **3**, 654–657 (2009).
30. Zhou, W. *et al.* Lasing action in strongly coupled plasmonic nanocavity arrays. *Nature Nanotech.* **8**, 506–511 (2013).
31. Gartia, M. R., Eichorst, J. P., Clegg, R. M. & Liu, G. L. Lifetime imaging of radiative and non-radiative fluorescence decays on nanoplasmonic surface. *Appl. Phys. Lett.* **101**, 023118 (2012).
32. Punj, D. *et al.* A plasmonic 'antenna-in-box' platform for enhanced single-molecule analysis at micromolar concentrations. *Nature Nanotech.* **8**, 512–516 (2013).
33. Consales, M. *et al.* Lab-on-fiber technology: Toward multifunctional optical nanoprobes. *ACS Nano* **6**, 3163–3170 (2012).
34. Garrett, C., Kaiser, W. & Bond, W. Stimulated emission into optical whispering modes of spheres. *Phys. Rev.* **124**, 1807–1809 (1961).
35. Lin, H. & Campillo, A. Microcavity enhanced Raman gain. *Opt. Commun.* **133**, 287–292 (1997).
36. Vollmer, F. & Arnold, S. Whispering-gallery-mode biosensing: label-free detection down to single molecules. *Nature Methods* **5**, 591–596 (2008).
37. Gerard, D. *et al.* Strong electromagnetic confinement near dielectric microspheres to enhance single-molecule fluorescence. *Opt. Express* **16**, 15297–15303 (2008).
38. Lin, H. & Campillo, A. CW nonlinear optics in droplet microcavities displaying enhanced gain. *Phys. Rev. Lett.* **73**, 2440–2443 (1994).
39. Ausman, L. K. & Schatz, G. C. Whispering-gallery mode resonators: Surface enhanced Raman scattering without plasmons. *J. Chem. Phys.* **129**, 054704 (2008).
40. Savchenkov, A. A., Matsko, A. B., Ilchenko, V. S. & Maleki, L. Optical resonators with ten million finesse. *Opt. Express* **15**, 6768–6773 (2007).
41. White, I., Oveys, H. & Fan, X. Increasing the enhancement of SERS with dielectric microsphere resonators. *Spectroscopy* **21**, 36–42 (2006).
42. Zou, S. & Schatz, G. C. Combining micron-size glass spheres with silver nanoparticles to produce extraordinary field enhancements for surface-enhanced Raman scattering applications. *Isr. J. Chem.* **46**, 293–297 (2006).
43. Spillane, S. M., Kippenberg, T. J. & Vahala, K. J. Ultralow-threshold Raman laser using a spherical dielectric microcavity. *Nature* **415**, 621–623 (2002).
44. Shopova, S. I., Blackledge, C. W. & Rosenberger, A. T. Enhanced evanescent coupling to whispering-gallery modes due to gold nanorods grown on the microresonator surface. *Appl. Phys. B-Lasers and Opt.* **93**, 183–187 (2008).
45. Fuller, K. A. & Smith, D. D. Cascaded photoenhancement from coupled nanoparticle and microcavity resonance effects. *Opt. Express* **15**, 3575–3580 (2007).
46. Grivas, C. *et al.* Single-mode tunable laser emission in the single-exciton regime from colloidal nanocrystals. *Nat. Commun.* **4**, 2376 (2013).
47. Choi, Y. *et al.* Ultrahigh-Q microsphere dye laser based on evanescent-wave coupling. *J. Kor. Phys. Soc.* **39**, 928–931 (2001).
48. White, I. M., Gohring, J. & Fan, X. SERS-based detection in an optofluidic ring resonator platform. *Opt. Express* **15**, 17433–17442 (2007).
49. Wu, X., Li, H., Liu, L. & Xu, L. Unidirectional single-frequency lasing from a ring-spiral coupled microcavity laser. *Appl. Phys. Lett.* **93**, 081105 (2008).
50. Kim, W., Safonov, V., Shalaev, V. & Armstrong, R. Fractals in microcavities: Giant coupled, multiplicative enhancement of optical responses. *Phys. Rev. Lett.* **82**, 4811–4814 (1999).
51. Siadat Mousavi, S., Berini, P. & McNamara, D. P. Periodic plasmonic nanoantennas in a piecewise homogeneous background. *Opt. Express* **20**, 18044–18065 (2012).
52. Yao, Y. *et al.* Broad electrical tuning of graphene-loaded plasmonic antennas. *Nano Lett.* **13**, 1257–1264 (2013).
53. Nie, S. & Emery, S. Probing single molecules and single nanoparticles by surface-enhanced Raman scattering. *Science* **275**, 1102–1106 (1997).
54. Ahn, W., Hong, Y., Boriskina, S. V. & Reinhard, B. M. Demonstration of efficient on-chip photon transfer in self-assembled optoplasmonic networks. *ACS Nano* **7**, 4470–4478 (2013).
55. Tomes, M. & Carmon, T. Photonic micro-electromechanical systems vibrating at X-band (11-GHz) rates. *Phys. Rev. Lett.* **102**, 113601 (2009).
56. Barth, M., Schietinger, S., Fischer, S., Becker, J., Nusse, N., Aichele, T., Lochel, B., Sonnichsen, C. & Benson, O. Nanoassembled plasmonic-photonic hybrid cavity for tailored light-matter coupling. *Nano Lett.* **10**, 891–895 (2010).
57. Devilez, A., Stout, B. & Bonod, N. Compact metallo-dielectric optical antenna for ultra directional and enhanced radiative emission. *ACS Nano* **4**, 3390–3396 (2010).
58. Boriskina, S. V. & Reinhard, B. M. Spectrally and spatially configurable superlenses for optoplasmonic nanocircuits. *Proc. Natl. Acad. Sci. U. S. A.* **108**, 3147–3151 (2011).
59. Santiago-Cordoba, M. A., Cetinkaya, M., Boriskina, S. V., Vollmer, M. F. & Demirel, M. C. Ultrasensitive detection of a protein by optical trapping in a photonic-plasmonic microcavity. *J. Biophotonics* **5**, 629–638 (2012).
60. Ahn, W., Boriskina, S. V., Hong, Y. & Reinhard, B. M. Photonic-plasmonic mode coupling in on-chip integrated optoplasmonic molecules. *ACS Nano* **6**, 951–960 (2012).
61. Shopova, S. I., Rajmangal, R., Holler, S. & Arnold, S. Plasmonic enhancement of a whispering-gallery-mode biosensor for single nanoparticle detection. *Appl. Phys. Lett.* **98**, 243104 (2011).
62. Hong, Y., Pourmand, M., Boriskina, S. V. & Reinhard, B. M. Enhanced light focusing in self-assembled optoplasmonic clusters with subwavelength dimensions. *Adv. Mater.* **25**, 115–119 (2013).
63. Kuwata-Gonokami, M. & Takeda, K. Polymer whispering gallery mode lasers. *Opt. Mater.* **9**, 12–17 (1998).
64. Xu, Z., Chen, Y., Gartia, M. R., Jiang, J. & Liu, G. L. Surface plasmon enhanced broadband spectrophotometry on black silver substrates. *Appl. Phys. Lett.* **98**, 241904 (2011).
65. Oxborrow, M. Traceable 2D finite-element simulation of the whispering-gallery modes of axisymmetric electromagnetic resonators. *IEEE Trans. Microw. Theory Tech.* **55**, 1209–1218 (2007).
66. Cornell, S. & Koenig, J. Laser-excited Raman scattering in polystyrene. *J. Appl. Phys.* **39**, 4883–& (1968).
67. Troccoli, M. *et al.* Raman injection laser. *Nature* **433**, 845–848 (2005).
68. Fagnano, C., Fini, G. & Torreggiani, A. Raman-spectroscopic study of the Avidin-Biotin complex. *J. Raman Spectrosc.* **26**, 991–995 (1995).

69. Venkateswaran, C. S. & Pandya, N. S. The Raman spectra of organic compounds: Diethyl disulphide. *Proc. Indian Acad. Sci. - Section A* **15**, 396–400 (1942).

70. Neish, C. S., Martin, I. L., Henderson, R. M. & Edwardson, J. M. Direct visualization of ligand-protein interactions using atomic force microscopy. *Br. J. Pharmacol.* **135**, 1943–1950 (2002).

71. van Munster, E. & Gadella, T. Fluorescence lifetime imaging microscopy (FLIM). *Microscopy Techniques* **95**, 143–175 (2005).

## Author contributions

M.R.G., G.L.L. and J.G.E. designed the project and organized the entire research program. M.R.G. and J.G.E. wrote the manuscript. M.R.G. carried out the sample preparation and characterization. S.S. performed the FDTD simulation. J.K. performed the COMSOL simulation. T.W.C. performed the SEM characterization. G.B. supervised the COMSOL simulation and FEM modelling. M.L. performed the protein and dye conjugation. M.L. provided the reagents and wrote the protocol for the protein conjugation. M.R.G. and J.G.E. analyzed the Raman scattering results. All authors discussed the results and commented on the manuscript.

## Additional information